

論文 / 著書情報  
Article / Book Information

Title	Centrifuge study on the effect of the SCP improvement geometry on the mitigation of liquefaction-induced embankment settlement
Authors	Yang Li, Masaki Kitazume, Akihiro Takahashi, Kenji Harada, Jun Ohbayashi
Citation	Soil Dynamics and Earthquake Engineering, Vol. 148, 106852
Pub. date	2021, 9
DOI	<a href="http://dx.doi.org/10.1016/j.soildyn.2021.106852">http://dx.doi.org/10.1016/j.soildyn.2021.106852</a>
Creative Commons	See next page.
Note	This file is author (final) version.

# License



Creative Commons: CC BY-NC-ND

1 **Title:**  
2 Centrifuge study on the effect of the SCP improvement geometry on the mitigation of  
3 liquefaction-induced embankment settlement  
4

5 **Authors:**  
6 Yang Li  
7 Department of Civil and Environment Engineering, Tokyo Institute of Technology, Japan  
8 2-12-1 Ookayama, Meguro-Ku, 152-8552 Tokyo, Japan  
9 E-mail address: ri.y.ac@m.titech.ac.jp  
10

11 Masaki Kitazume  
12 Department of Civil and Environment Engineering, Tokyo Institute of Technology, Japan  
13 2-12-1 Ookayama, Meguro-Ku, 152-8552 Tokyo, Japan  
14 E-mail address: kitazume.m.aa@m.titech.ac.jp  
15

16 Akihiro Takahashi  
17 Department of Civil and Environment Engineering, Tokyo Institute of Technology, Japan  
18 2-12-1 Ookayama, Meguro-Ku, 152-8552 Tokyo, Japan  
19 E-mail address: takahashi.a.al@m.titech.ac.jp  
20

21 Kenji Harada  
22 Geo-Technical Division, Fudo Tetra Corporation, Japan  
23 7-2, Nihonbashi-Koami-chou, Chuou-ku, Tokyo 103-0016, Japan  
24 E-mail address: kenji.harada@fudotetra.co.jp  
25

26 Jun Ohbayashi  
27 Geo-Technical Division, Fudo Tetra Corporation, Japan  
28 7-2, Nihonbashi-Koami-chou, Chuou-ku, Tokyo 103-0016, Japan  
29 E-mail address: jun.ohbayashi@fudotetra.co.jp  
30

31 **Soil Dynamics and Earthquake Engineering, 148, 106852, 2021**

32 **Official URL:** <https://doi.org/10.1016/j.soildyn.2021.106852>  
33

34 **Keywords:**  
35 liquefaction countermeasure, sand compaction pile, improvement geometry, centrifuge test  
36

37 **Abstract:**

38 Liquefaction of foundation soil causes significant damage to infrastructures. The sand compaction  
39 pile (SCP) method is a countermeasure against liquefaction to densify the ground by installing  
40 dense sand piles. In recent years, an innovative method has been developed to install sand piles  
41 into the ground at any angle. In this study, a series of dynamic centrifuge tests are carried out to  
42 investigate the effects of the angle of the SCP improvement zone on mitigating the liquefaction-  
43 induced settlement of embankment crests. The lateral displacement beneath the embankment toes  
44 is mitigated by the presence of the improvement zone installed in the foundation ground. In  
45 particular, the case with a 50° improvement zone is the most effective in mitigating lateral  
46 displacement and contributes to the lower settlement of the embankment.

47

48 **1. Introduction**

49 During an earthquake, saturated loose sandy soil is characterized by a substantial rise in excess  
50 pore water pressure, leading to a drastic loss of its strength and stiffness. When the excess pore  
51 water pressure reaches the initial effective overburden stress, soil particles do not support each  
52 other, and liquefaction takes place, which usually causes severe damage, such as cracking,  
53 slumping, lateral spreading and settlement, to river dykes, levees and road embankments. For  
54 instance, many embankments and river dykes that failed due to the liquefaction of foundation  
55 ground were reported during the 1964 Alaskan and Niigata earthquake [1], [2], the 1983  
56 Nipponkai-Chubu, Japan earthquake [3], and the 1995 Hyogoken-Nambu, Japan earthquake [4],  
57 among many others. During the 2011 Great East Japan earthquake, more than 2000 locations of  
58 embankments suffered some level of damage caused by liquefaction of the foundation ground [5].  
59 Soil liquefaction and related damage to earthen structures have been extensively studied by many  
60 researchers in past decades [6]–[10]. It was reported that the primary cause of embankment  
61 settlement was the lateral deformation of liquefied soil beneath the embankment away from the  
62 embankment center.

63 To date, many liquefaction countermeasures based on various principles have been developed  
64 (e.g., densification, deep mixing, drainage). Among them, the SCP method is a typical ground  
65 densification method, which has often been applied to mitigate liquefaction to densify the ground  
66 by installing vertical compacted sand piles into the ground. The SCP method is considered to  
67 increase ground density and uniformity [11]. The effectiveness of the SCP method as a  
68 countermeasure against liquefaction has been confirmed in past earthquakes, including the 1978  
69 Miyagi-Oki earthquake [12], showing that this method is one of the most reliable ground  
70 improvement methods in Japan [13]. It is also expected to be applied to the ground improvement  
71 of civil engineering structures in the future.

72 On the other hand, there are numerous existing soil structures worldwide that were either

73 constructed before the seismic design standard was established or without it [14]. To prevent  
74 potential damage to these existing structures from liquefaction in future earthquakes, it may be  
75 necessary to remediate the foundation soil. However, the conventional SCP method constructing  
76 sand piles in the vertical direction is not able to densify ground underneath an existing structure.  
77 As mentioned above, during earthquake loading, most of the structural settlements and  
78 deformations are caused by the lateral movement of liquefied soils under the structure. To apply  
79 the SCP method to existing embankment structures, countermeasures are designed to provide  
80 confinement to the liquefied foundation soils moving away from the embankment centerline  
81 toward the free field, for which well-compacted sand piles are constructed under embankment  
82 toes in current practice. It has been reported that the occurrence of excessive settlement associated  
83 with large lateral deformation of liquefied foundation soils could be prevented effectively by this  
84 method; however, some embankment crest settlement was inevitable due to the deformation of  
85 liquefied sand under the embankment and volumetric strain with excess pore pressure dissipation  
86 under the embankment [15]–[18].

87 With advancements in machinery, a new type of SCP method has been recently developed, the  
88 SAVE-SP method, which enables the vertical installation of sand piles or the installation of sand  
89 piles at a specific angle into the ground. As the machine for this method is small, compacted sand  
90 piles can be formed in any direction underneath a structure, which is expected to prevent  
91 liquefaction and associated settlement more effectively [19], [20]. In addition, in previous studies,  
92 Yoshida et al. [21] performed shaking table tests where wooden sticks instead of sand piles were  
93 installed into the loose sand layer under residential houses at vertical and inclined angles. It was  
94 found that the wooden sticks installed at an inclined angle were more effective than those installed  
95 at a vertical angle. Rasouli et al. [22], [23] conducted 1 g model tests to evaluate the effect of  
96 sheet-pile walls as a countermeasure around the building's foundation and that combined with  
97 installing inclined drains under the structure. It was observed that the settlement and tilting of the  
98 building are reduced significantly in combination with inclined drains under the structure due to  
99 the installation of drains providing an area of nonliquefied ground under the building edges.

100 The geometric form of the improvement zones may affect the response and deformation behavior  
101 of the improved ground. However, these influences are not well investigated and incorporated  
102 into the current design precisely. The reliable and performance-based design of the new SCP  
103 method for embankments requires a clear understanding of the effect of various parameters that  
104 influence performance. In this study, four dynamic centrifuge experiments are carried out to  
105 investigate the effects of the angle of the SCP improvement zones on the liquefaction-induced  
106 deformation and response of the ground.

107

## 108 2. Centrifuge test program

109 A series of dynamic centrifuge tests are conducted to evaluate the effectiveness of SCP-improved  
110 ground with various geometric improvement forms and to investigate the effects of the geometry  
111 of the improved zone on the ground response and deformation mechanism of embankments and  
112 foundation ground. In the centrifuge test program, the focus is on the angle of the improvement  
113 zone, which is defined as the angle between the SCP improvement form and the ground base, in  
114 which the angle is changed from 50 to 90 degrees. Dynamic centrifuge tests are carried out  
115 utilizing the Tokyo Tech Mark III centrifuge facility [24] with a radius of 2.45 m at a centrifugal  
116 acceleration of 50 g. The model configurations and the entire test results are presented in prototype  
117 scale units unless indicated otherwise.

118

### 119 2.1 Design and description of centrifuge models

120 Four dynamic centrifuge tests are conducted on three different angles of the improvement zone  
121 over 50 to 90 degrees, as well as the benchmark model without any improvement. The model  
122 configurations are shown in Fig. 1 and Table 1. All tests simulate a prototype soil deposit of 7.5  
123 m depth and an embankment of 2.5 m height with a 1:2 slope. Case 1 constitutes the benchmark  
124 model under the typical condition that an embankment is supported by saturated loose sandy  
125 ground without any ground improvement. In Case 2, the vertical SCP improvement zones are  
126 placed under the embankment toes, which represents a conventional liquefaction remediation  
127 design for the existing embankment. Cases 3 and 4 simulate the improved ground using the new  
128 type of SCP method, where the densified improvement zones are constructed at the angles of 60  
129 and 50 degrees within the foundation ground. It should be noted here that the SCP improvement  
130 zone modeled in this study is not the same as the real condition of SCP improved ground. As  
131 shown in Fig. 2(a), in the practical design of SCP-improved ground, the interval of SCPs is  
132 determined based on the targeted density of the ground, and the extent of SCP improvement will  
133 be determined to ensure the stability of the embankment [25]. In practice, the SCP improvement  
134 zone is considered a composite ground consisting of dense SCPs and adjacent soil densified by  
135 SCPs. In this study, the SCP improvement zone is modeled by a uniform sand block with a relative  
136 density  $D_r = 90\%$  for easy model preparation. To determine the extent of the SCP improvement  
137 zone in the centrifuge experiment, preliminary experiments were conducted. Since this study  
138 focuses on the effect of the angle of SCP on mitigating embankment settlement, the extent of the  
139 SCP improvement zone is set to be large (5 m at the proto scale) so that the obvious effect can be  
140 confirmed.

141

### 142 2.2 Model preparation

143 A rigid container with inner dimensions of 600×150×400 mm is used in the tests. The front of

144 the rigid container has a transparent window, which enables observation of the model ground in  
145 the container during the experiment. Toyoura sand is used in the tests for the foundation and the  
146 improvement zone, whose properties are shown in Table 2.

147 In Case 1, the uniform sand ground is made by the air pluviation method to the relative density,  
148  $D_r \approx 50\%$ . The sand is poured through the air from a hopper, while the falling height is kept  
149 constant to obtain the desired relative density. In Cases 2, 3, and 4, the SCP improvement zones  
150 are made by tamping with 10% water content to  $D_r \approx 90\%$  first and then freezing. The front  
151 window of the container is disassembled, and the frozen soil blocks are placed at predetermined  
152 positions, as shown in Fig. 3. The remaining unimproved portions are filled with sand by air  
153 pluviation to the relative density,  $D_r \approx 50\%$ . DL clay, which consists of 90% silt and 10% clay, is  
154 mixed with 22% silicon oil by weight to build the embankments, having a unit weight of  $18 \text{ kN/m}^3$ .  
155 After the foundation ground is constructed, the embankment is carefully placed on the foundation  
156 ground at the desired place. The model ground is saturated with a mixture of water and 2%  
157 Metolose (hydroxypropyl methylcellulose) by weight of water to achieve a viscosity of  
158 approximately 50 times the viscosity of water. The purpose of using Metolose solution is to ensure  
159 the compatibility of the prototype permeability of the soil and to set up the affinity between  
160 dynamic and diffusion scaling laws [26]. The deaired Metolose solution is dripped slowly from  
161 the top of the container to the ground surface under vacuum conditions, which is continued until  
162 the water table reaches the top surface of the foundation ground. This saturation process requires  
163 approximately 48 hours.

164 Accelerometers and pore pressure transducers are installed as shown in Fig. 1 during the model  
165 preparation. They are installed to measure the accelerations and excess pore water pressure ( $\Delta u$ )  
166 at three regions representing different stress states: (1) free field, defined as the region that is  
167 unaffected by the embankment load; (2) under the embankment toe where static shear stress  
168 exists; and (3) under the center of the embankment where large effective stress exists.  
169 Potentiometers are set at the embankment crest to measure the crest settlement during the  
170 experiment, and a laser displacement transducer is placed at the embankment toe to measure the  
171 horizontal displacement of the embankment toe. The spaghetti noodle sticks are installed at  
172 predetermined positions between the foundation ground and the glass window of the container.  
173 After model saturation, the noodles become soft and act as markers that are used to map  
174 deformation patterns and magnitudes within the foundation ground.

175

### 176 2.3 Centrifuge test description

177 All the models are subjected to sinusoidal waves two times with a dominant frequency of 1 Hz,  
178 where the acceleration amplitude of the first shaking is approximately 150 gal and that of the  
179 second shaking is approximately 220 gal. Fig. 4 shows the acceleration time histories of input

180 base motions for Case 1 and Arias intensities of input base shakings for all cases for comparison.  
181 It is recognized from Fig. 4 that there is no noticeable difference in input motions between each  
182 case. The second shaking is imparted after full dissipation of pore water pressure in the foundation  
183 ground. Table 1 summarizes the model ground conditions and the peak acceleration of input  
184 motions in each case. After completion of the tests, each model is carefully inspected to measure  
185 the final locations of noodles for mapping the deformed shape.

186

### 187 3. Test results and discussion

#### 188 3.1 Excess pore water pressure and settlement responses

189 Figures 5-8 present time histories of the excess pore water pressures and settlements of the  
190 embankment crest for four cases during the first and second shakings. All the test results shown  
191 in the following sections are on the prototype scale unless mentioned otherwise. The excess pore  
192 water pressure (EPWP) is measured at several representative locations, as shown in Fig. 1. The  
193 evolution of EPWP plays a vital role in the understanding of liquefaction phenomena. The initial  
194 effective vertical stress at the relevant location is plotted with a horizontal dashed line in the  
195 figures ( $r_u = 1$  line). The initial vertical effective stresses due to embankment loading are  
196 calculated based on the influence values assuming the foundation ground to be elastic semi-  
197 infinite, as proposed by Osterberg [27]. Soils at a certain depth undergo liquefaction if the excess  
198 pore water pressure reaches the initial vertical effective stress ( $r_u = 1$  line). The ends of the  
199 shakings are indicated with vertical dashed lines in the figures.

200 The EPWP time histories during the first shaking event of  $A_{\max} \approx 150$  gal are presented in Fig.  
201 5. In the free field of the benchmark model (Case 1), the EPWP at W6 (at a depth of 2.0 m) attains  
202 the initial effective vertical stress indicated by the  $r_u=1$  line at 25 s after the base shaking starts  
203 and that at W3 (at a depth of 5.5 m) reaches the  $r_u=1$  line at 30 s, corresponding to the condition  
204 of sand liquefaction at these regions. These results demonstrate that the liquefaction of the sand  
205 layer in the free field starts near the ground surface and propagates downward. Under the  
206 embankment toe, the EPWP at W5 reaches the  $r_u = 1$  line at almost the same time with the same  
207 depth in the free field (W6). Unfortunately, the pore water pressure transducer W2 did not work  
208 correctly because of the EPWP beyond the measurable range from 25 s to 90 s, but it is presumed  
209 from measured data that the EPWP at W2 also reaches the  $r_u=1$  line at approximately 30 s, which  
210 means that liquefaction also occurred under the embankment toes during the first shaking in Case  
211 1. Beneath the embankment center, a low EPWP is observed at a depth of 2.0 m (W4), with a  
212 significant reduction in EPWP during shaking (from approximately 25 s). The EPWP at the deeper  
213 portion under the center of the embankment (W1) is generated to the same value as that in the  
214 free field at the same depth (W3), but the EPWP does not reach the  $r_u=1$  line. Such lower EPWP  
215 values beneath the embankment were also reported by other centrifuge and 1 g tests [9], [15], [28].

216 The deviatoric stress induced by the embankment surcharge is a beneficial component that  
217 prevents the buildup of EPWP during shaking. Furthermore, the rapid liquefaction in the free field  
218 might have reduced the confinement (horizontal effective stress) of the soil below the  
219 embankment, leading to the soil below the embankment tending to move laterally away due to  
220 large induced shear stress. This mechanism dictates the soil dilation, resulting in a reduction in  
221 the EPWP. In addition, some RPI researchers have reported that drainage is more significant in  
222 the sand layer under higher confining pressure[29]–[31]. The SCP improvement zone is  
223 considered to provide higher confinement of the soil under the embankment. Therefore, it may  
224 enhance the faster drainage of the soil under the embankment.

225 In Case 2, improved by 90° improvement zones below the embankment toes; unfortunately, the  
226 pore water pressure transducers W3 and W6 indicated that the EPWP in the free field did not work  
227 correctly from 25 s because of the EPWP was beyond the measurable range. However, it is  
228 presumed from the measured data that the situation of the free field in Case 2 is similar to Case 1  
229 in terms of liquefaction that occurred in those regions. At W5 beneath the embankment toe, similar  
230 EPWP behavior is observed to that in Case 1, which indicates that liquefaction also occurs below  
231 the embankment toes in Case 2. Unfortunately, the pore water pressure transducer W2 in Case 2  
232 did not work because of some unforeseen reasons and hence is not shown in Fig. 5. Under the  
233 embankment centerline, the EPWP at the deeper portion (W1) is very similar to that in Case 1.  
234 However, different behavior is observed at the shallower portion beneath the embankment center  
235 (W4) between Case 2 and Case 1. There is no reduction in EPWP at W4 in Case 2 during the first  
236 shaking. This may be attributed to the smaller horizontal deformation beneath the embankment  
237 center due to the confinement of the improvement zones.

238 On the other hand, quite different responses of EPWP are observed in Case 3 and Case 4 during  
239 the first shaking compared to the above two cases. In Case 3, which has inclined improvement  
240 zones with 60° angles under the embankment, even though there is no significant difference in  
241 the input acceleration between each case (see Fig. 4(b)), the EPWP at W6 in the free field is  
242 generated fast at the beginning of shaking but decreases immediately, although shaking continues.  
243 Similar EPWP responses are also observed at the deeper portion in the free field (W3), below the  
244 embankment toe (W2 and W5) and under the embankment center (W1 and W4). This EPWP  
245 response is not clear, but one possible reason is that the pore pressures propagate to the  
246 improvement zones very quickly due to the large pressure difference between the improvement  
247 zone and surrounding sand. In Case 4, the EPWP at W6 is observed to be similar to that in Case  
248 1 during shaking, which indicates that liquefaction occurred in the free field near the ground  
249 surface. Unfortunately, W3 did not work correctly from 25 s. Under the embankment toe, at W5,  
250 the EPWP starts to increase at the beginning of shaking but decreases immediately, as observed  
251 in Case 3. However, at W2, a high EPWP is generated, which reaches the  $r_u=1$  line but dissipates

252 immediately during shaking. The EPWP under the embankment center in Case 4 is very similar  
253 to that observed in Case 3.

254 Settlements measured at the embankment crest (P1, shown in Fig. 1) during the first shaking are  
255 shown in Fig. 6. In the benchmark model Case 1, the settlement begins with the EPWP increasing  
256 within the foundation ground (10-25 s) and increases rapidly when liquefaction occurs below the  
257 embankment toe and in the free field from 25 s (see Fig. 5). A relatively large embankment crest  
258 settlement of approximately 0.38 m is measured. Essentially, almost all of this settlement takes  
259 place during shaking. The settlement response in Case 2 is very similar to that in Case 1 until 35  
260 s during shaking due to the similar EPWP responses in Cases 1 and 2. In contrast, the settlement  
261 rate is decreased from 35 s during shaking, which is considered due to the effectiveness of the  
262 vertical improvement zones under the embankment toes for mitigating the lateral displacement of  
263 the ground below the embankment, which will be discussed in Subsection 3.3. On the other hand,  
264 a significantly small amount of settlements is observed in Cases 3 and 4. Because of the  
265 significantly lower EPWP values below the embankment in these two cases, the stiffness of the  
266 ground below the embankment in Cases 3 and 4 does not degrade significantly during the first  
267 shaking. It is expected that the free field response is not influenced by the embankment and the  
268 boundary effect of the container side. However, the space of the container used in this study is  
269 limited. Then, some influence from the embankment and container side on the free field response  
270 was unavoidable because a sufficient distance could not be secured. As Fig. 5 shows, the EPWPs  
271 generated under the embankment in Cases 3 and 4 are very low compared to those in Cases 1 and  
272 2. The author believes that even though the EPWP responses in the free field in Cases 3 and 4  
273 become similar to those in Cases 1 and 2, and the settlement result does not change much during  
274 the first shaking. For the sake of brevity, it is not shown in this paper, but the sensitivity analysis  
275 by finite element analysis showed that the EPWP response in the free field could be different  
276 depending on the container width, while its impact on the deformation of the foundation ground  
277 under the embankment was not significant.

278 Figure 6 shows the EPWP time histories during the second shaking event of  $A_{\max} \approx 220$  gal. The  
279 responses of EPWP in Case 1 and Case 2 are almost the same as those during the first shaking,  
280 i.e., liquefaction occurs below the embankment toe and in the free field, whereas the soil under  
281 the center of the embankment does not reach a liquefaction state, but high EPWP is generated at  
282 the deeper portion. During the second shaking, in Cases 3 and 4, liquefaction occurs below the  
283 embankment toe and in the free field, caused by the large cyclic shear stress induced by the larger  
284 shaking. It is worth noting that the EPWPs at the deeper portion under the center of the  
285 embankment in Cases 3 and 4 seem to be larger than those in Cases 1 and 2. However, the EPWP  
286 values at the shallower portion (at W4) in Cases 3 and 4 are smaller than those in Cases 1 and 2.  
287 This may be because the deeper portion is liquefied during the shaking period and prevents the

288 waves from propagating upward. Regarding the higher excess pore water pressure generated  
289 under the embankment in the improved ground, similar behavior was also observed in other  
290 centrifuge experiments and numerical analyses [17], [18], [32], where the ground under the  
291 embankment toes improved by SCPs as well as the deep mixing method and sheet pile. The higher  
292 excess pore water pressure may be partly due to the horizontal deformation suppressed by the  
293 SCP improvement zone, resulting in the soils under the embankment showing a contractive  
294 response (i.e., generation of EPWP).

295 Figure 7 depicts the settlement time histories of the embankment crest during the second shaking.  
296 Herein, it should be noted that the ground conditions of the cases are altered due to the first  
297 shaking. Particularly, in Case 1 and Case 2, the density of the soil below the embankment should  
298 have become denser than that before being subjected to the first shaking because of considerable  
299 settlement during the first shaking. Additionally, the gradients of the embankment slope in Case  
300 1 and Case 2 are less than those before the first shaking, which indicates a reduction in shear  
301 stress within the ground induced by the embankment. In Case 1, excessive settlement is also  
302 observed during the second shaking. In Case 2, the settlement starts at a lower rate in comparison  
303 with Case 1, when liquefaction occurs within the ground. In Cases 3 and 4, less settlement is  
304 observed in comparison with Case 1, and settlement ceases faster in Case 4 compared to Case 3,  
305 which suggests that a 50° improvement (Case 4) is more effective in mitigating the embankment  
306 settlement in comparison with a 60° improvement (Case 3).

307 There are two types of ground deformation that contribute to liquefaction ground settlement:  
308 shear deformation and volumetric change [33]. Figs. 6 and 8 show that most of the settlements  
309 occurred during shaking and that those after shaking were very small, which indicates that  
310 volumetric change due to drainage occurred during shaking. The average volumetric strains of  
311 the ground under the embankment in each case after shaking were confirmed by the measured  
312 volume change under the embankment. In addition, 1% to 2.5% of the volumetric strains were  
313 found within the ground under the embankment. The following effects of these volumetric strains  
314 on the behavior of excess pore water pressure and settlement are considered. One is that the  
315 amount of settlement due to drainage is approximately 1% to 2.5%, including the amount of  
316 settlement during shaking. Therefore, compared with the completely undrained condition, the  
317 result of the settlement presented here is slightly overestimated. Another is that if the ground is  
318 under completely undrained conditions, the excess pore water pressure may be generated faster  
319 than that under drained conditions. As a result, it is possible that the amount of settlement due to  
320 shear deformation of the ground will be larger.

321

322

323 3.2 Distribution of maximum excess pore pressures under the embankment

324 Figures 8 and 9 illustrate the distribution of the maximum EPWP with depth under the  
325 embankment center and toe subjected to the first and second shakings, respectively. It should be  
326 noted that the maximum EPWP values indicated in Figs. 8 and 9 are the monotonic components  
327 picked up from the EPWP time histories. The dashed lines in the figure represent the initial  
328 vertical effective stress with depth. These figures are plotted to clarify the extent of liquefaction  
329 in different cases during each shaking event. In the first shaking, as shown in Fig. 9, the maximum  
330 EPWP values do not reach the initial vertical effective stress under the embankment center in all  
331 cases, which means that the soil under the embankment centerline is not liquefied even though  
332 the values of the maximum EPWP are different between each case. The effect of the improvement  
333 angle on the EPWP values will be discussed later using Fig. 11. Beneath the embankment toe, at  
334 a depth of 2.0 m, the maximum EPWP in Case 1 and Case 2 reaches the initial effective stress,  
335 indicating that liquefaction occurs beneath the toes in these two cases. At the same location, the  
336 maximum EPWP values in Cases 3 and 4 are below the initial effective stress line, indicating that  
337 the soil is not liquefied beneath the toes in these two cases during the first shaking.

338 Figure 9 shows the maximum EPWP distribution for all cases during the second shaking event  
339 ( $A_{max} \approx 220$  gal). Under the embankment center, the maximum EPWP at the deeper portion (at a  
340 depth of 5.5 m) tends to be a similar value in all cases, among which the improved ground cases  
341 (i.e., Case 2, Case 3, and Case 4) showed higher EPWPs than the unimproved ground case. At the  
342 shallower portion (at a depth of 2.0 m), the EPWPs in all cases stay at much lower values than  
343 the initial effective stress. Beneath the embankment toe, the soils are considered liquefied  
344 irrespective of the ground conditions because the EPWPs in all cases at this location reach the  
345 initial effective stress.

346 As mentioned that the EPWP plays a vital role in the liquefaction phenomena and related effects,  
347 it is motivated to evaluate the effect of the angle of improvement zone on the generation of EPWP  
348 within the ground. To achieve this, Fig. 11 depicts the relationship between the angle of the  
349 improvement zone and the maximum EPWP at the representative locations within the ground  
350 subjected to the first and second shakings.

351 During the first shaking event (see Fig. 11(a)), the response in the free field seems almost the  
352 same irrespective of the angle of the improvement, since the values have no variation along the  
353 angle of the improvement zone. Beneath the embankment toe, the maximum EPWPs generated  
354 in the cases with 50 and 60 degree improvement zones are smaller than those in the cases without  
355 improvement and with 90 degree improvement zones. The same trend is also observed beneath  
356 the embankment center (see the black lines in Fig. 11(a)), especially at the deeper portion below  
357 the embankment center, where the EPWP values measured in Cases 3 and 4 are approximately  
358 20% of the values measured in Cases 1 and 2. Overall, during the first shaking with a relatively  
359 smaller acceleration amplitude, a lower EPWP is observed in Cases 3 and 4 than in Cases 1 and

360 2, except in the free field.

361 The results of each case for the second shaking are shown in Fig. 11(b). In the free field, it seems  
362 that there is no relation to the angle of the improvement. A similar trend is observed beneath the  
363 toe. In other words, there is no significant influence of the degree of improvement zone on the  
364 maximum EPWP in the free field and beneath the toe. However, under the embankment center,  
365 the maximum EPWP at a deeper portion (at a depth of 5.5 m) is larger in the improvement cases,  
366 especially in Cases 3 and 4. This trend is the opposite of the situation in the first shaking. At the  
367 shallower portion beneath the embankment center, the maximum EPWP generated in Cases 3 and  
368 4 is smaller than that in Cases 1 and 2, which is the same trend as that in the first shaking.

369

### 370 3.3 Lateral displacement beneath embankment toe

371 As mentioned in the introduction, the major cause of the embankment settlement induced by  
372 liquefaction of the foundation ground is the lateral displacement of liquefied soil beneath the  
373 embankment away from the embankment center. Countermeasures in the remediation program  
374 for embankments, therefore, aim at mitigating crest settlement by providing confinement to the  
375 liquefiable foundation soils by forming remediated stiff zones in the liquefiable soil layer under  
376 embankment toes. To evaluate the effectiveness of the improvement zone with a different angle,  
377 the lateral displacement beneath the embankment toe is discussed in this subsection.

378 Fig. 12 depicts the lateral displacement distribution beneath the embankment toe after the first  
379 and second shakings. In Fig. 12, the dashed lines present the results after the first shaking, and  
380 the solid lines present those after the second shaking. It should be noted that the displacement  
381 distributions after the second shaking contain the displacement produced during the first shaking.

382 After the first shaking, the lateral displacement in Case 1 is observed with a maximum value of  
383 approximately 0.2 m at a depth of 2.0 m and decreases toward the ground surface and base. In  
384 Case 2, the shape of lateral displacement distribution beneath the toe is similar to Case 1, but the  
385 amount of displacement was mitigated compared to that in Case 1 below a depth of 1.5 m. In Case  
386 3 and Case 4, the lateral displacements are significantly smaller than the other two cases, which  
387 is attributed to the lower EPWP generation during the first shaking (see Figs. 5 and 9).

388 After the second shaking, a significant increment of lateral displacement is observed in Case 1  
389 at the whole depth, especially at depths from 1.0 to 3.5 m. This might be because the EPWP  
390 remains lower at the shallower portion beneath the center of the embankment (see Figs. 9 and 10),  
391 and then the soil in that portion does not lose the strength and stiffness significantly. Whereas, the  
392 EPWP at the deeper portion is high. Then, a large lateral displacement of sand can be expected  
393 below the portion where EPWP remains lower beneath the embankment. A similar deformation  
394 mechanism was also reported in other studies [34]–[36]. The lateral displacement in Case 2 also  
395 increases during the second shaking due to liquefaction occurring again beneath the toe and in the

396 free field (see Fig. 7), but the amount is smaller than that in Case 1. In Cases 3 and 4, the increment  
397 of lateral displacements is observed after the second shaking, caused by liquefaction that occurred  
398 during the second shaking. Although a high EPWP is generated at the deeper portion below the  
399 embankment during the second shaking (see Fig. 10), the lateral displacement at the deeper  
400 portion seems mitigated more effectively in Cases 3 and 4 than in the cases without improvement  
401 and with a 90 degree improvement zone.

402 From the above results, it is suggested that the main mechanism responsible for the settlement  
403 of the embankment is the form of soil softening due to a decrease in effective stresses (generation  
404 of EPWP) in the foundation ground, permitting vertical compression to accompany lateral  
405 displacement. In this study, the ground improved by 50° angle improvement zones is the most  
406 effective for mitigating the lateral displacement.

407 To evaluate the effect of different improvement angles on mitigating lateral displacement  
408 quantitatively, the area of the lateral displacement distribution along the depth (i.e., the amount of  
409 laterally deformed soil) is calculated from the distribution shown in Fig. 12. Fig. 13 presents the  
410 relationship between the angle of the SCP improvement zone and the area of lateral displacement.  
411 During the first shaking, the overall lateral displacement in Cases 3 and 4 is significantly smaller  
412 than that in Cases 1 and 2 due to the much lower EPWP generated in Cases 3 and 4 compared to  
413 the other two cases (see Fig. 11(a)). During the second shaking, in all cases, the amount of total  
414 lateral displacement is more than that after the first shaking. This might be due to the liquefaction  
415 state sustaining a longer time than the first shaking (see Figs. 5 and 7). Overall, Fig. 13 confirms  
416 the effectiveness of the inclined improvement zone in mitigating lateral displacement. Among  
417 them, the improvement with the 50° angle case shows the best performance.

418

#### 419 3.4 Settlement beneath the embankment

420 As mentioned in section 3.1, some extent of drainage under the embankment might occur during  
421 shaking, even though undrained conditions are aimed at in the model test. According to the  
422 measured volume change under the embankment, the drainage effect on the ground settlement is  
423 small. Several centrifuge tests (e.g., [15]) and shaking table tests at 1 g (e.g., [37]) have been  
424 conducted to explore the effectiveness of remedial countermeasures beneath embankment toes  
425 for reducing crest settlement. The above-referenced studies showed that embankment crest  
426 settlement after shaking was greater than half of the settlement in the case without  
427 countermeasures, although the lateral displacements beneath the toes were significantly mitigated  
428 with a countermeasure. One reason for this is that the embankment settlement contains the  
429 shaking-induced compression of the embankment itself. To eliminate this component from the  
430 embankment settlement, a comparison of the settlement below the embankment is also useful.

431 Figure 14 depicts the settlement distribution at the embankment bottom after the first and second

432 shakings. In Fig. 14, the dashed lines present the results after the first shaking, and the solid lines  
433 present the results after the second shaking. In Case 1, the bottom of the embankment is settled  
434 overall, where the largest settlement occurred under the crest and decreased toward the toe for  
435 both the first and second shakings. In Case 2, the difference compared to Case 1 is that the soil  
436 shows an upward heave near the toe. It might be that the lateral displacement constraint is imposed  
437 by the vertical improvement zone, resulting in formations of a low strength exit path near the toes  
438 where liquefaction occurred (see Figs. 9 and 10). This deformation pattern would lead to an  
439 increase in the settlement under the crest. The same observation was also reported by the other  
440 centrifuge tests (e.g., [16], [22]). In Case 3, the soil beneath the toe also heaves but is smaller than  
441 that in Case 2. In Case 4, no significant heave deformation near the toe is observed. This might  
442 be due to the presence of stiff improvement zones below the toes, and the volume of the  
443 deformable soil below the toes decreases. This effect should be significant in Case 4, as there is a  
444 larger improvement area below the toes.

445

### 446 3.5 Settlement of embankment crest

447 Figure 15 plots the vertical displacement of the embankment crest (P1 shown in Fig. 1) against  
448 the angle of the improvement zone immediately after the first and second shakings, as well as the  
449 settlement due to the dissipation of EPWP after shaking. In every shaking event, the difference  
450 between settlement immediately after shaking and that after dissipation of EPWP is very small,  
451 which demonstrates that the main settlement occurs during shaking.

452 In Fig. 15, the shape of the lines is very similar to that shown in Fig. 13, which indicates that the  
453 relationship between the angle of the improvement zone and the area of lateral displacement has  
454 a one-to-one relationship. It is verified that there is a strong correlation between the lateral  
455 displacement beneath the toes and the settlement of the embankment. Additionally, it is suggested  
456 that the improvement conditions that can mitigate lateral displacement more effectively are also  
457 effective in mitigating embankment settlement. It is clear from Fig. 15 that all improvement cases  
458 show the effectiveness of mitigating embankment crest settlement. Among them, Case 4 improved  
459 by a 50° angle is the most effective in mitigating the settlement, which is considered to be because  
460 the lateral displacement beneath the toes is most mitigated in comparison with other cases.

461

## 462 4. Conclusions

463 A series of dynamic centrifuge tests are carried out to investigate the effects of the angle of the  
464 SCP improvement zone on mitigating the liquefaction-induced settlement of embankment crests.  
465 The following major conclusions are drawn from the test results:

- 466 (1) The excess pore water pressure (EPWP) responses in the ground are influenced by the angle  
467 of the improvement zone. During small shaking (150 gal), the maximum EPWP under the

468 embankment center and near the toe in the case of the 60° and 50° improvement zones is less  
469 than that in the unimprovement case and 90° improvement case. During the larger shaking  
470 (220 gal), the maximum EPWP under the embankment center at the deep layer tends to  
471 become higher values in the 60° and 50° improvement zones in comparison with the  
472 unimprovement case and 90° improvement case. At a shallower portion of the foundation  
473 ground under the embankment center, the trend of the maximum EPWP is similar to that  
474 during small shaking, but there is a marginal difference between cases under the toe.

475 (2) It is confirmed that the lateral displacement beneath the embankment toes is mitigated by the  
476 presence of the improvement zone installed in the foundation ground. In particular, the case  
477 with a 50° improvement zone is the most effective and contributes to the lower settlement of  
478 the embankment.

479 (3) The deformation pattern of the soil below the embankment toe is also important for the  
480 mitigation of crest settlement. In the case with the 90° improvement zone, a relatively larger  
481 heave is observed beneath the embankment toe, whereas in the 60° and 50° improvement  
482 cases, such heave deformation near the toe is suppressed. Since this heave deformation  
483 beneath the toe makes the crest settlement larger, it is suggested that in addition to lateral  
484 displacement beneath the embankment toe, the deformability of the soil under the  
485 embankment toe is also important for mitigating the crest settlement of the embankment.

486

#### 487 References

- 488 [1] D. McCulloch and M. Bonilla, "Railroad damage in the Alaska Earthquake," *J. Soil*  
489 *Mech. Found. Div.*, vol. 93, no. SM5, pp. 89–100, 1967, [Online]. Available:  
490 <http://trid.trb.org/view.aspx?id=126871>.
- 491 [2] F. Kawakami and A. Asada, "Damage to the ground and earth structures by the Niigata  
492 earthquake of June 16, 1964," *soils Found.*, vol. 6, no. 1, pp. 14–30, 1966, doi:  
493 10.1248/cpb.37.3229.
- 494 [3] S. Tani, "Consideration of Earthquake Damage to Earth Dam for Irrigation in Japan," in  
495 *Proceedings of the 2nd International Conference on Recent Advances in Geotechnical*  
496 *Earthquake Engineering and Soil Dynamics*, 1991, pp. 1137–1142.
- 497 [4] S. Tani, "Damage to earth dams," *Soils Found.*, vol. Special, pp. 263–272, 1996.
- 498 [5] F. Oka, P. Tsai, S. Kimoto, and R. Kato, "Damage patterns of river embankments due to  
499 the 2011 off the Pacific Coast of Tohoku Earthquake and a numerical modeling of the  
500 deformation of river embankments with a clayey subsoil layer," *Soils Found.*, vol. 52,  
501 no. 5, pp. 890–909, 2012, doi: 10.1016/j.sandf.2012.11.010.
- 502 [6] H. B. Seed and I. M. Idriss, "Simplified Procedure For Evaluating Soil Liquefaction  
503 Potential," *J. soil Mech. Found. Div.*, vol. 97, no. SM9, pp. 1249–1273, 1971.

- 504 [7] H. B. Seed, "Landslides during earthquakes due to soil liquefaction," *J. Geotech. Eng.*,  
505 vol. 94, pp. 1055–1123, 1968.
- 506 [8] Y. Sasaki *et al.*, "Mechanism of permanent displacement of ground caused by seismic  
507 liquefaction," *soils Found.*, vol. 32, no. 3, pp. 79–96, 1992.
- 508 [9] Y. Koga and O. Matsuo, "Shaking table tests of embankments resting on liquefiable  
509 sandy ground," *Soils Found.*, vol. 30, no. 4, pp. 162–174, 1990.
- 510 [10] O. Matsuo, "Damage to river dikes," *soils Found.*, vol. Special, pp. 235–240, 1996.
- 511 [11] M. Kitazume, *The Sand Compaction Pile Method*. 2005.
- 512 [12] K. Ishihara, Y. Kawase, and M. Nakajima, "Liquefaction characteristics of sand deposits  
513 at an oil tank site during the 1978 Miyagiken-oki earthquake," *Soils Found.*, vol. 20, no.  
514 2, pp. 97–111, 1980.
- 515 [13] K. Harada and J. Ohbayashi, "Development and improvement effectiveness of sand  
516 compaction pile method as a countermeasure against liquefaction," *Soils Found.*, vol. 57,  
517 no. 6, pp. 980–987, 2017, doi: 10.1016/j.sandf.2017.08.025.
- 518 [14] H. Mitrani and S. P. G. Madabhushi, "Cementation liquefaction remediation for existing  
519 buildings," *Gr. Improv.*, vol. 163, no. 2, pp. 81–94, 2010, doi:  
520 10.1680/grim.2010.163.2.81.
- 521 [15] K. Adalier, A.-W. Elgamal, and G. R. Martin, "Foundation liquefaction countermeasures  
522 for earth embankments," *J. Geotech. Geoenvironmental Eng.*, vol. 124, no. 6, pp. 500–  
523 517, 1998.
- 524 [16] M. Okamura and O. Matsuo, "Effects of remedial measures for mitigating embankment  
525 settlement due to foundation liquefaction," *IJPMG-International J. Phys. Model.*  
526 *Geotech.*, vol. 2, pp. 1–12, 2002.
- 527 [17] M. Okamura and K. Tamura, "Prediction method for liquefaction-induced settlement of  
528 embankment with remedial measure by deep mixing method," *soils Found.*, vol. 44, no.  
529 4, pp. 53–65, 2004.
- 530 [18] A. Elgamal, E. Parra, Z. Yang, and K. Adalier, "Numerical analysis of embankment  
531 foundation liquefaction countermeasures," *J. Earthq. Eng.*, vol. 6, no. 4, pp. 447–471,  
532 2002.
- 533 [19] M. Kitazume, A. Takahashi, K. Harada, and N. Shinkawa, "New type sand compaction  
534 pile method for densification of liquefiable ground underneath existing structure," *J.*  
535 *Geo-Engineering Sci.* 3, pp. 1–13, 2016, doi: 10.3233/JGS-150032.
- 536 [20] Y. Li, M. Kitazume, A. Takahashi, K. Harada, and J. Ohbayashi, "Dynamic FEM  
537 analyses on behavior of SCP improved ground with various geometry," *Japanese*  
538 *Getechnical J.*, vol. 14, no. 2, pp. 161–178, 2019.
- 539 [21] M. Yoshida, M. Miyajima, and A. Numata, "Experimental Study on Liquefaction

- 540 Countermeasure Technique by Log Piling for Residential Houses,” 2012.
- 541 [22] R. Rasouli, I. Towhata, and T. Akima, “Experimental Evaluation of Drainage Pipes as a  
542 Mitigation against Liquefaction-Induced Settlement of Structures,” *J. Geotech.*  
543 *Geoenvironmental Eng.*, vol. 142, no. 9, p. 04016041, 2016, doi:  
544 10.1016/j.jcline.2008.08.024.
- 545 [23] R. Rasouli, I. Towhata, H. Rattez, and R. Vonaesch, “Mitigation of Nonuniform  
546 Settlement of Structures due to Seismic Liquefaction,” *J. Geotech. Geoenvironmental*  
547 *Eng.*, vol. 144, no. 11, p. 04018079, 2018, doi: 10.1061/(ASCE)GT.1943-5606.0001974.
- 548 [24] J. Takemura, M. Kondoh, T. Esaki, M. Kouda, and O. Kusakabe, “Centrifuge model  
549 tests on double propped wall excavation in soft clay,” *soils Found.*, vol. 39, no. 3, pp.  
550 75–87, 1999.
- 551 [25] K. Harada and J. Ohbayashi, “Development and improvement effectiveness of sand  
552 compaction pile method as a countermeasure against liquefaction,” *Soils Found.*, vol. 57,  
553 no. 6, pp. 980–987, 2017, doi: 10.1016/j.sandf.2017.08.025.
- 554 [26] G. Madabhushi, *Centrifuge modelling for civil engineering*. CRC Press, 2014.
- 555 [27] J. Osterberg, “Influence values for vertical stresses in semi-infinite mass due to  
556 embankment loading,” in *Proceedings of the 4th international conference on soil*  
557 *mechanics and foundation engineering*, 1957, pp. 393–396.
- 558 [28] B. Mehrzad, Y. Jafarian, C. J. Lee, and A. H. Haddad, “Centrifuge study into the effect  
559 of liquefaction extent on permanent settlement and seismic response of shallow  
560 foundations,” *Soils Found.*, vol. 58, no. 1, pp. 228–240, 2018, doi:  
561 10.1016/j.sandf.2017.12.006.
- 562 [29] W. El-Sekelly, R. Dobry, T. Abdoun, and M. Ni, “Numerical Simulation of the Effect of  
563 High Confining Pressure on Drainage Behavior of Liquefiable Clean Sand,” *J. Geotech.*  
564 *Geoenvironmental Eng.*, vol. 146, no. 12, p. 04020131, 2020, doi:  
565 10.1061/(asce)gt.1943-5606.0002381.
- 566 [30] M. Ni, T. Abdoun, R. Dobry, K. Zehtab, A. Marr, and W. El-Sekelly, “Pore Pressure and  
567  $K_{\sigma}$  Evaluation at High Overburden Pressure under Field Drainage Conditions. I:  
568 Centrifuge Experiments,” *J. Geotech. Geoenvironmental Eng.*, vol. 146, no. 9, p.  
569 04020088, 2020, doi: 10.1061/(asce)gt.1943-5606.0002303.
- 570 [31] T. Abdoun, M. Ni, R. Dobry, K. Zehtab, A. Marr, and W. El-Sekelly, “Pore Pressure and  
571  $K_{\sigma}$  Evaluation at High Overburden Pressure under Field Drainage Conditions. II:  
572 Additional Interpretation,” *J. Geotech. Geoenvironmental Eng.*, vol. 146, no. 9, p.  
573 04020089, 2020, doi: 10.1061/(ASCE)GT.1943-5606.0002302.
- 574 [32] S. Bhatnagar, S. Kumari, and V. A. Sawant, “Numerical Analysis of Earth Embankment  
575 Resting on Liquefiable Soil and Remedial Measures,” *Int. J. Geomech.*, vol. 16, no. 1, p.

- 576 04015029, 2016, doi: 10.1061/(ASCE)GM.1943-5622.0000501.
- 577 [33] J. M. Pestana *et al.*, “Mechanisms of Seismically Induced Settlement of Buildings with  
578 Shallow Foundations on Liquefiable Soil Mechanisms of Seismically Induced Settlement  
579 of Buildings with Shallow Foundations on Liquefiable Soil,” *J. Geotech.*  
580 *Geoenvironmental Eng.*, vol. 136, no. 1, pp. 151–164, 2010, doi:  
581 10.1061/(ASCE)GT.1943-5606.0000179.
- 582 [34] K. Kawasaki, T. Sakai, S. Yasuda, and M. Satoh, “Earthquake-induced settlement of an  
583 isolated footing for power transmission tower,” in *Centrifuge 98*, 1998, pp. 271–276.
- 584 [35] B. Ghosh, “Behaviour of Rigid Foundation in Layered Soils During Seismic  
585 Liquefaction,” *PhD thesis, Department of Engineering, University of Cambridge*. 2003.
- 586 [36] O. Adamidis and S. P. G. Madabhushi, “Deformation mechanisms under shallow  
587 foundations on liquefiable layers of varying thickness,” *Géotechnique*, pp. 1–12, 2017,  
588 doi: 10.1680/jgeot.17.P.067.
- 589 [37] M. Nasu, H. Fujisawa, and K. Hikimoto, “An experimental study on prevention of  
590 embankment deformation due to liquefaction of sandy ground,” *Q. Rep. Railw. Tech.*  
591 *Res. Inst.*, vol. 28, no. 1, pp. 5–6, 1987.
- 592
- 593

594 **List of Tables**

595 Table 1: Summary of test conditions

596 Table 2: Index properties of Toyoura sand

597

598

599 **List of figures**

600 Fig. 1: Model configurations: (a) Case 1: unimproved ground, (b) Case 2: 90° improvement zones,  
601 (c) Case 3: 60° improvement zones, (d) Case 4: 50° improvement zones

602 Fig. 2: Simplification of the SCP improvement zone modeled in the centrifuge experiment

603 Fig. 3: Photographs of model ground preparation (Case 4)

604 Fig. 4: (a) Acceleration time histories of input base motions for Case 1, (b) Arias intensities of  
605 input base shakings for all cases

606 Fig. 5: Excess pore water pressure time histories during the first shaking

607 Fig. 6: Settlement time histories of the embankment crest during the first shaking

608 Fig. 7: Excess pore water pressure time histories during the second shaking

609 Fig. 8: Settlement time histories of the embankment crest during the second shaking

610 Fig. 9: Maximum excess pore pressure profiles during the 1st shaking ( $A_{\max} \approx 150$  gal)

611 Fig. 10: Maximum excess pore pressure profiles during the 2nd shaking ( $A_{\max} \approx 220$  gal)

612 Fig. 11: Relation between angle of improvement zone and maximum EPWP within the ground (at  
613 W1, W4, W5 and W6), (a) during first shaking, (b) during second shaking

614 Fig. 12: Lateral displacement beneath the embankment toe (after first and second shaking)

615 Fig. 13: Relationship between the angle of the SCP remedial zone and the area of lateral  
616 deformation

617 Fig. 14: Vertical displacement of the ground under embankment

618 Fig. 15: Relationship between the angle of the SCP remedial zone and vertical displacement

Table 1 Summary of test conditions

Test code	Model description	Peak acceleration of input motion (gal)	
		First shaking	Second shaking
Case 1	Sand foundation without any improvement	150	220
Case 2	Vertical SCP improvement zone	140	210
Case 3	60 degrees SCP improvement zone	140	220
Case 4	50 degrees SCP improvement zone	140	240

Table 2 Index properties of Toyoura sand

Property	Value
Specific gravity, $G_s$	2.65
$D_{50}$ (mm)	0.19
$D_{10}$ (mm)	0.14
Maximum void ratio, $e_{max}$	0.973
Minimum void ratio, $e_{min}$	0.609
Permeability, $k$ (m/s) at $Dr=50\%$	$2 \times 10^{-4}$
Permeability, $k$ (m/s) at $Dr=90\%$	$1.5 \times 10^{-5}$

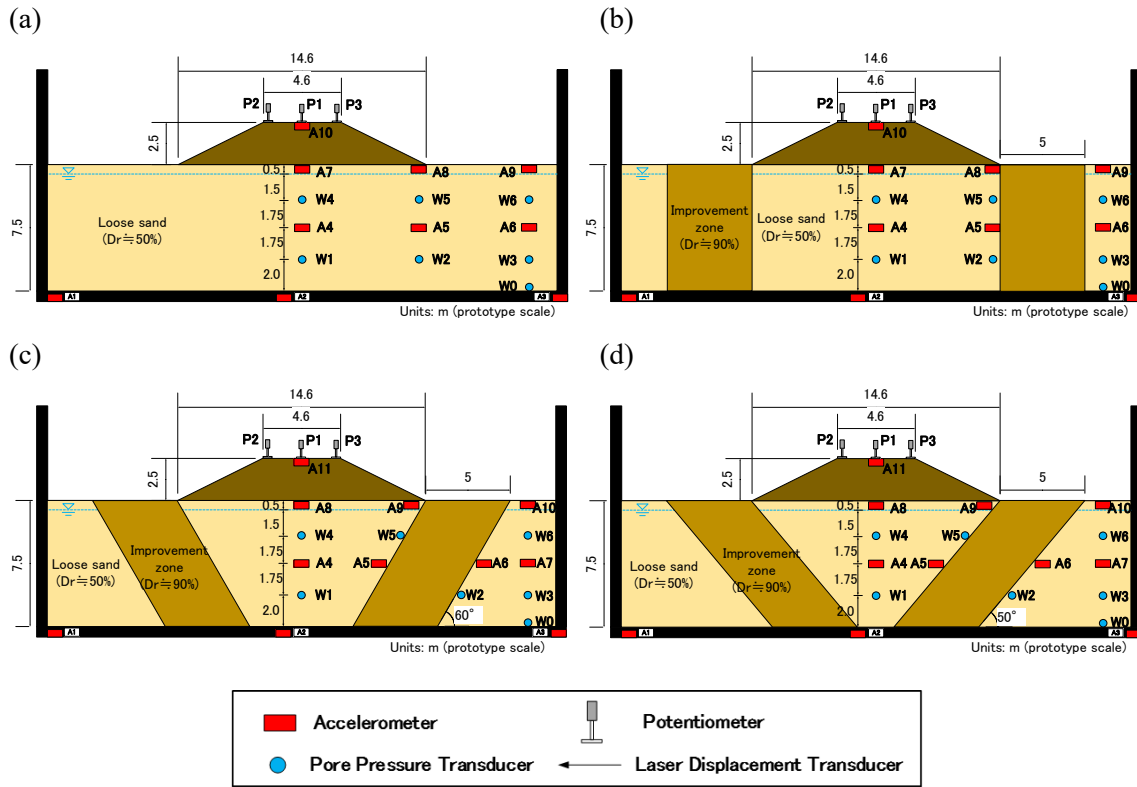


Fig. 1. Model configurations: (a) Case 1: unimproved ground, (b) Case 2:  $90^\circ$  improvement zones, (c) Case 3:  $60^\circ$  improvement zones, (d) Case 4:  $50^\circ$  improvement zones

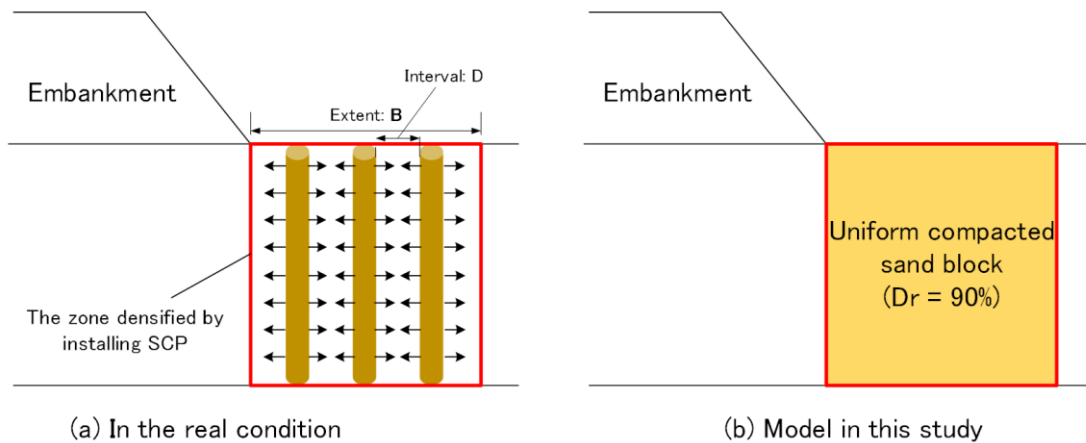


Fig. 2. Simplification of the SCP improvement zone modeled in the centrifuge experiment

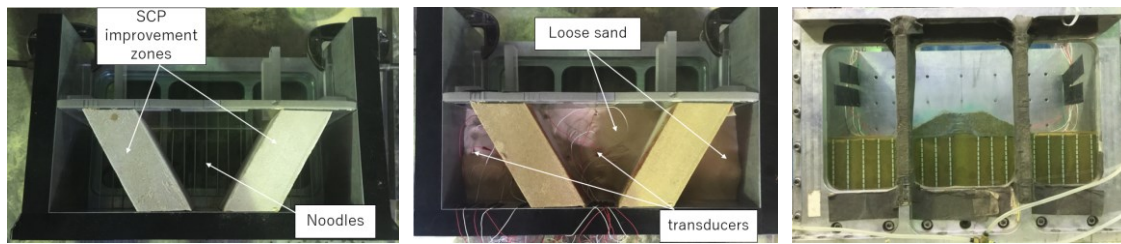


Fig. 3. Photographs of model ground preparation (Case 4)

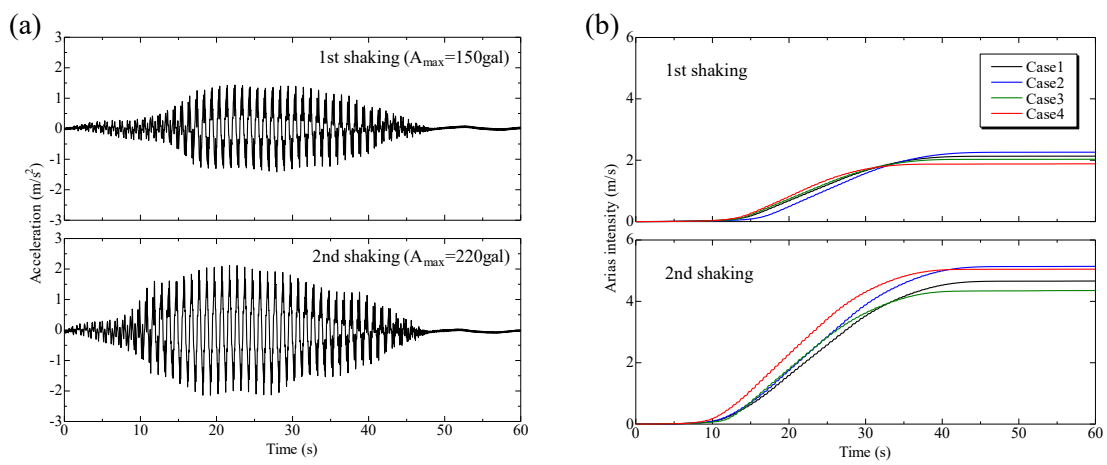


Fig. 4. (a) Acceleration time histories of input base motions for Case 1, (b) Arias intensities of input base shakings for all cases

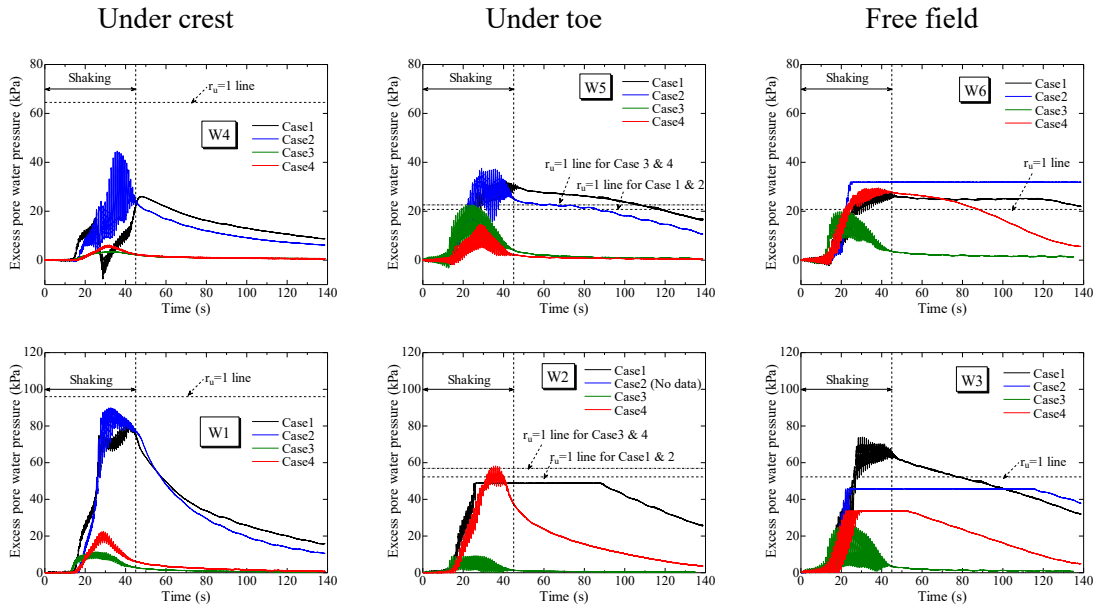


Fig. 5. Excess pore water pressure time histories during first shaking

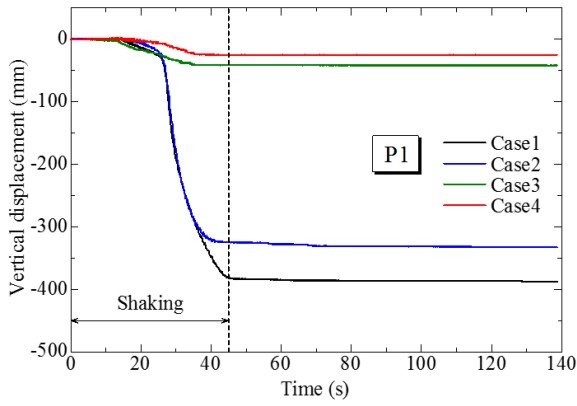


Fig. 6. Settlement time histories of the embankment crest during the first shaking

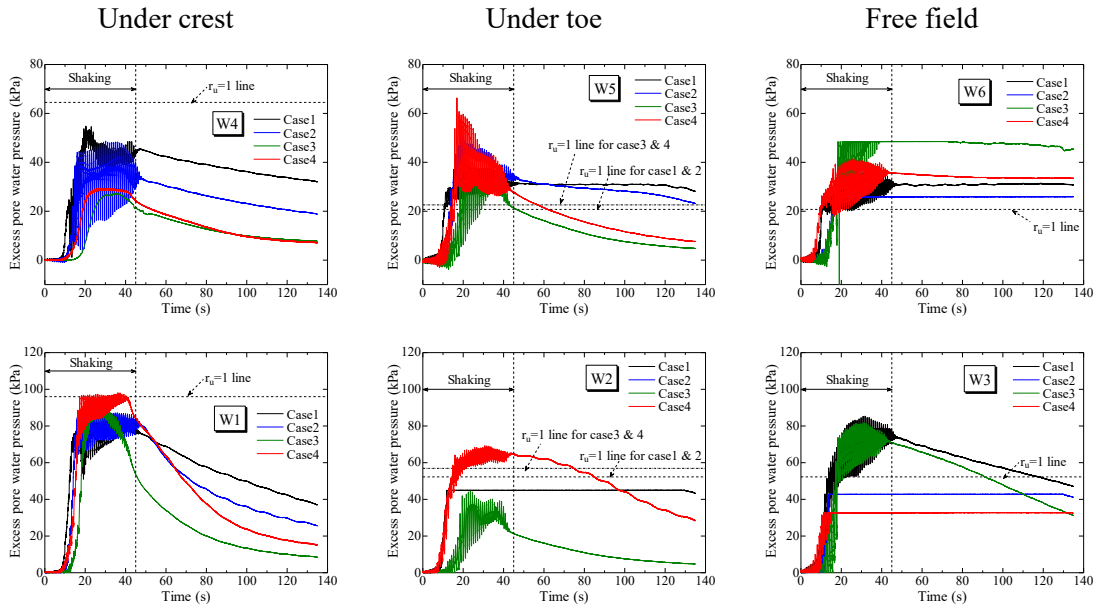


Fig. 7. Excess pore water pressure time histories during second shaking

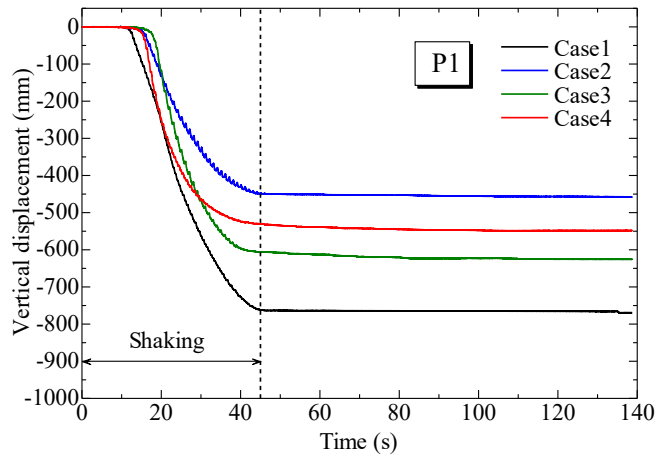


Fig. 8. Settlement time histories of the embankment crest during the second shaking

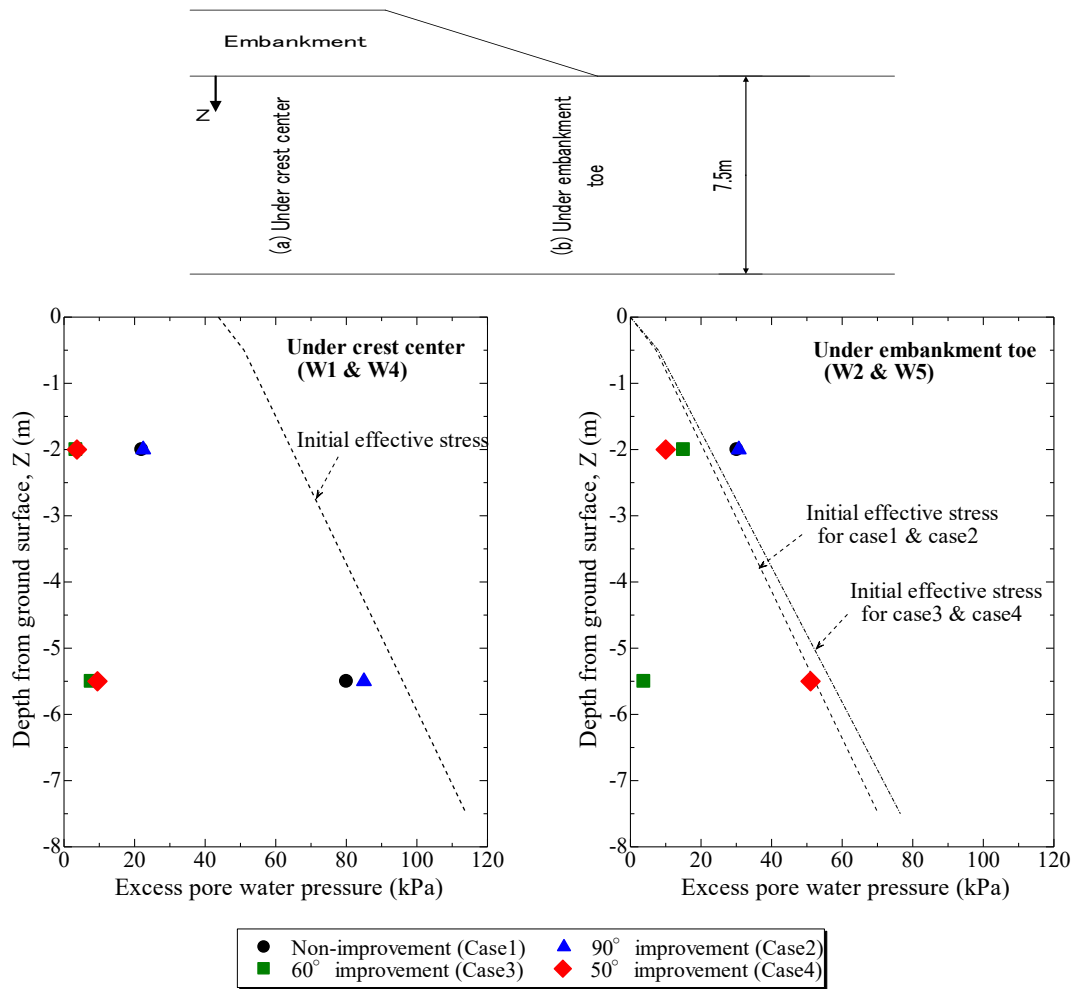


Fig. 9. Maximum excess pore pressure profiles during 1st shaking ( $A_{max} \approx 150$  gal)

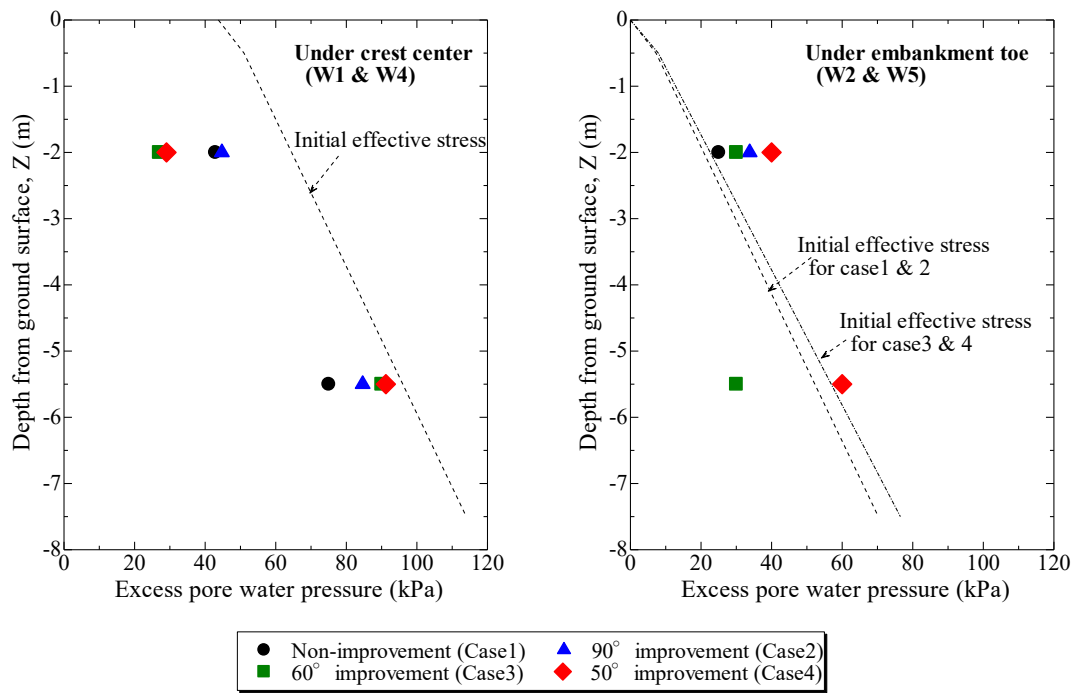


Fig. 10. Maximum excess pore pressure profiles during 2nd shaking ( $A_{max} \approx 220$  gal)

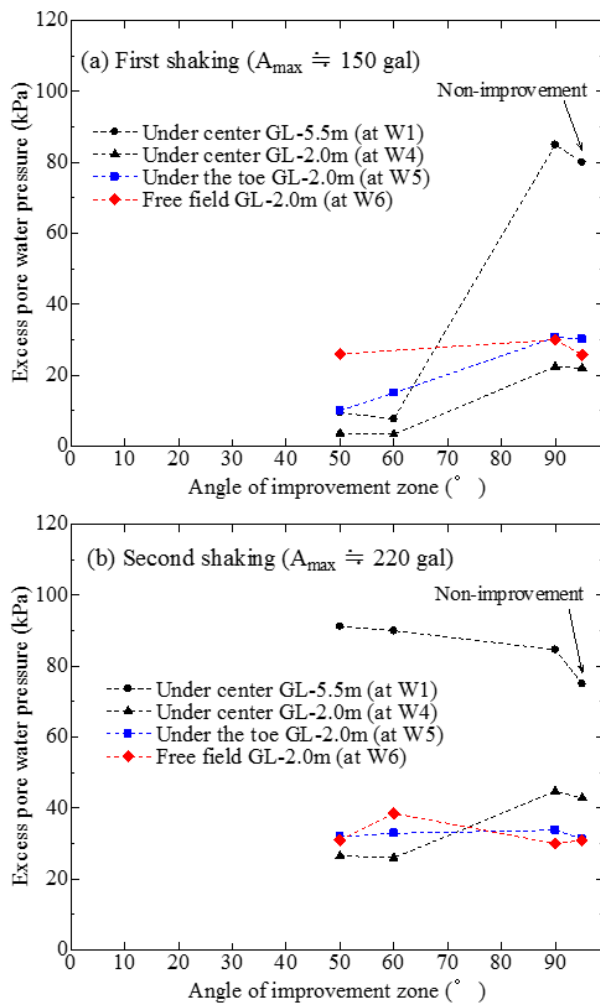


Fig. 11. Relationship between angle of improvement zone and maximum EPWP within the ground (at W1, W4, W5 and W6), (a) during first shaking, (b) during second shaking

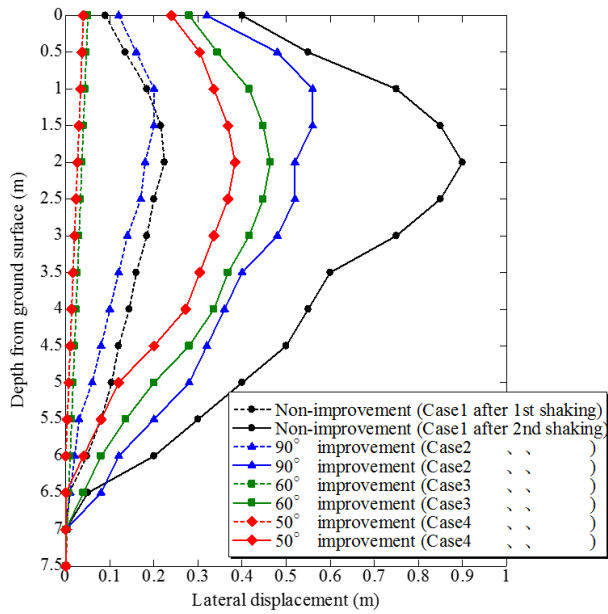


Fig. 12. Lateral displacement beneath the embankment toe (after first and second shaking)

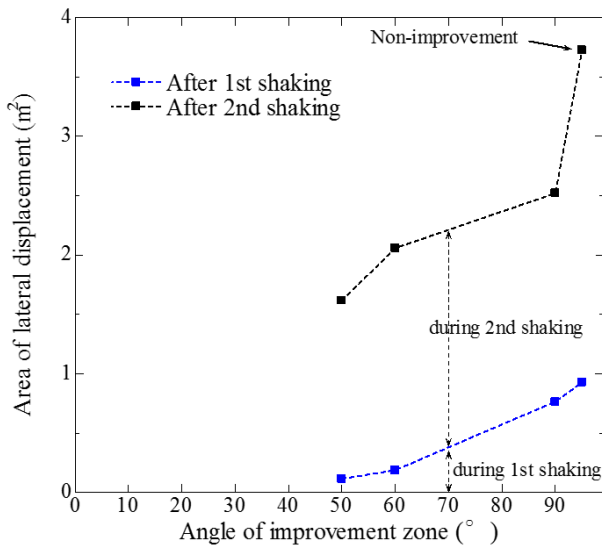


Fig. 13. Relationship between the angle of SCP remedial zone and area of lateral deformation

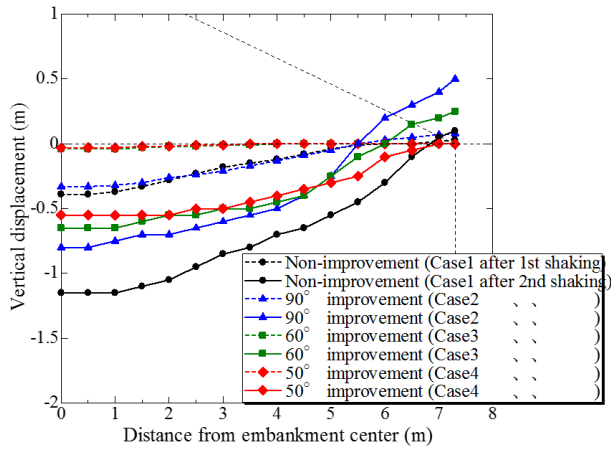


Fig. 14. Vertical displacement of the ground under embankment

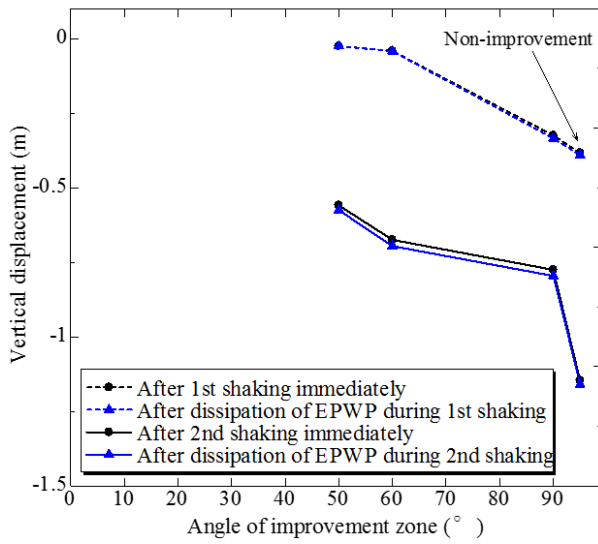


Fig. 15. Relationship between angle of SCP remedial zone and vertical displacement